Voter model emergence in stem cell niche homeostasis

Author: Joan Térmens Cascalló
*Facultat de Física, Universitat de Barcelona, Diagonal 645, 08028 Barcelona, Spain.**

Advisor: Marta Ibañes Miguez

Abstract: Recent studies suggest that homeostasis could be maintained in stem cell niches by collective cell dynamics rather than by asymmetric cell division. Here we study the collective cell dynamics that lead to an homeostasis maintenance in stem cell niches, the well-known critical birth-death model (CBD) and the voter model (VM), as well as a feedback model in which cell fate (proliferation or differentiation) is determined stochastically by local density. For the feedback case, the system is simulated with three cell motion dynamics: non-interacting, growth-migration and growth-adhesion. We find that for all motion dynamics the system starts to evolve as the CBD whereas VM emerges at long times and length scales for short-ranged dynamics. Long-ranged dynamics do not exhibit VM emergence.

I. INTRODUCTION

In most adult tissues, cells that are damaged or die get replaced by stem cells that differentiate and become part of the tissue. This replacement mechanism requires a population of stem cells in homeostasis throughout the adult life. To maintain homeostasis (i.e. constant cell density) a balance between stem cell proliferation and differentiation is needed [1].

For a great portion of adult tissues it continues to be unclear how stem cell populations achieve and regulate this precise balance [2]. To explain it, asymmetric cell division has been proposed [3]. This way, a stem cell divides into a differentiated cell and a daughter stem cell. Strong evidences of this mechanism have been found in invertebrates, with numerous studies in *C. elegans* and *Drosophila* [4]. However, some recent papers [5–8] have found that in some mouse tissues this mechanism is not at play and instead stem cells divide frequently and are lost and replaced by neighbouring cells in a stochastic way [2]. Thus, homeostasis is reached as a collective phenomena rather than by single-cell processes of asymmetric cell division.

This paradigm of collectively reached homeostasis is characterized by three properties [2]. Firstly, the average number of cells per clone (i.e. the group of descendant cells of a certain cell) shows a power-law growth ($n_{surv}(t) \sim t^{\delta}$). Secondly, the number of remaining clones at a certain time decreases inversely proportional to the growth of the clone, and third, cumulative clone size distributions, that is the probability of having no less than n cells in a certain clone, exhibits the scaling behaviour $C_n(t) \sim \Phi[n/n_{surv}(t)]$ [2, 9]. In regards of clone size statistics it is possible to distinguish between two main canonical behaviours, the so called critical birth-death process (CBD) [10] and the voter model (VM) [11–14].

The CBD reflects cell-intrinsic regulation [2] and considers all stem cells as independent units with equal probability of either proliferation and differentiation [9]. The non-interacting CBD kinetics describe a mean-field dynamics, which results in the scaling form $\delta = 1$ and $\Phi(X) = e^{-X}$ [8], independent of system's dimension. On the other hand, the VM reflects cell-extrinsic regulation [2] and considers that the proliferation of a cell is triggered by the differentiation of a neighbouring cell, resulting this time in the scaling form $\delta = 1/2$ and $\Phi(X) = e^{-\pi X^2/4}$ for 1-dim systems [2, 9] and $\delta = 1$ (with logarithmic correction) and $\Phi(X) = e^{-X}$ for 2-dim systems [2, 14]. Although CBD dynamics have not been experimentally observed, studies in 1-dim stem cell niches had found consistent experimental results with the VM in intestinal crypts [5], male germ line [6] and oral epithelium [7]. Evidences of VM emergence had been found in some 2-dim tissues like the epidermis [8] too. The finding of VM in male germ line stem cell niches is specially interesting due to the high motility and sparsely distribution of the germ line cells which extensively differs from the classical VM examples in a lattice or continuum.

Here, both cell-intrinsic regulation (CBD) and cell-extrinsic regulation (VM) scenarios are numerically simulated and its scaling behaviours are reproduced. Additionally, we propose a version a model of cell fate decision (i.e. the choice between proliferation or differentiation at the end of a cell's lifetime) proposed in [9, 13] in which CBD and VM behaviours emerge as a consequence of a density feedback in the cell fate dynamics [9]. This feedback model is simulated within three different cell motion dynamics: non-interacting (NI), growth-migration (GM) and growth-adhesion (GA) coupling.

II. MODEL

A. Modeling the canonical examples

For the critical birth-death process (CBD) each cell begins with a random exponential lifetime with mean t_{cell},

*Electronic address: joan.termens@gmail.com

that is the average cell lifetime at homeostasis, and a random fate (either proliferation or differentiation with probability 1/2). At each iteration, the cell with a minor remaining lifetime is selected. Then, if the selected cell has the fate of differentiation, it simply leaves the niche and, otherwise, the cell proliferates such that two new cells will replace it. A random exponential lifetime with mean t_{cell} and a random fate is assigned to both daughter cells. It is important to note that all cells have equally distributed lifetimes (exponential with mean t_{cell}) and fates (1/2 proliferation and 1/2 differentiation) at any time.

On the other hand, the voter model (VM) has been simulated assigning a random exponential lifetime with mean t_{cell} to each cell. At each iteration the cell with a minor remaining lifetime is differentiated and replaced by the proliferation of a neighbouring cell, which is chosen at random with equal probability (1/2) to both neighbours. A random exponentially distributed lifetime with mean t_{cell} is assigned to each descendant and the other cell's lifetimes are updated.

Note that these models only include cell fate dynamics.

B. Density feedback model

Lastly, we seek to obtain a model in which the two previous behaviours emerge from cell-cell interaction and via a feedback as in [9, 13]. In this version of the model presented in [9, 13], the stem cell niche is described as a self-replicating N-body Langevin system with cell-cell interactions and a field dependant feedback. The idea is that different field's configurations let to different cell lifetimes and fates. This fields could include the local density [9], the homeostatic pressure [15], the concentration of growth factor [13], stress and effects from other cells, such as signaling. For simplicity, we restrict the feedback to a local density dependence [9]. More concretely, cells sense the local density around them and act accordingly, so although fate decisions remain stochastic, a low density will promote proliferation as well as a higher one, differentiation. We define local density as:

$$\rho_L(x;t) = \frac{1}{2L+1}\int_{x-L}^{x+L} \mathrm{d}x' \sum_{j=1}^{N(t)} \delta(x' - x_j(t)), \qquad (1)$$

where L stands as the interaction range. Small interaction ranges ($L \approx l_0$, where l_0 is the adult cell's size) can be achieved via mechanical cues whereas long ranges ($L \approx L_{sys}$) could be a consequence of autocrine signalling [9]. Because of this density feedback, both cell fate dynamics and cell motion dynamics need to be described.

1. *Cell fate dynamics*

Cell fate decisions are characterized by two density dependant rates, $\omega^{\pm}(\rho_L)$, with ω^+ being the proliferation rate and ω^- the differentiation one. The density at which both rates are equal, ρ_{ss}, is the system's density at homeostasis. For each stem cell, two stochastic lifetimes τ^+ and τ^- are computed from exponential distributions with rates $\omega^{\pm}(\rho_L)$, respectively. If $\tau^+ < \tau^-$ the cell will proliferate after time τ^+, while if $\tau^- < \tau^+$ the cell will differentiate after time τ^- [9].

As a first order approximation, we have considered a linear feedback [13] by setting

$$\omega^{\pm}(\rho_L) = \lambda\left(\mp r\frac{\rho_L - \rho_{ss}}{\rho_{ss}} + 1\right)\theta(\rho_c - \rho_L), \qquad (2)$$

where ρ_{ss} is the density at homeostasis and has been fixed at the equilibrium density $\rho_{ss} = 1/l_0$ (l_0 is the adult cell's size) and $\lambda = 1/t_{cell}$ is the average reaction rate at homeostasis with t_{cell} being the cell's mean life. $r > 0$ is a real parameter and ρ_c is a cutoff density, so for $\rho_L > \rho_c$, $\omega^{\pm}(\rho_L) = \omega^{\pm}(\rho_c)$.

2. *Cellular growth and motion dynamics*

When a cell proliferates it is substituted by two descendants that initially occupy the same space as the progenitor, so cells born with half its adult size, l_0. To reach its adult state both cells must grow until its size its equal to the adult size. We have approximated this growth by a linear model

$$\frac{\mathrm{d}}{\mathrm{d}t}l_j(t) = \frac{\Delta l}{t_{gr}} = \frac{l_0/2}{t_{gr}}, \qquad (3)$$

where l_j is the j-th cell size and $t_{gr} < t_{cell}$ is the growth time.

The spatial position of stem cells in the niche is modeled considering them as interacting particles labeled by $j \in \{1, 2, ..., N(t)\}$, where $N(t)$ is the number of cells at certain time t. In a 1-dim space, the equations of motion take the form of an overdamped Langevin system [9, 13]:

$$\frac{\mathrm{d}}{\mathrm{d}t}x_j(t) = -\frac{\partial}{\partial x_j}U(\{x\}) + \sqrt{2D}\eta_j(t), \qquad (4)$$

where D is the diffusion constant of a free cell and the potential term adds pairwise interactions between cells: $U(\{x\}) := \sum_{j=1}^{N(t)}\sum_{\langle j,k\rangle} u_{jk}$, with u_{jk} being a cell-cell adhesion potential and $\langle j,k\rangle$ indicating summation over the first neighbours of cell j. $\eta_j(t)$ denotes independent white noise, $\langle\eta_j(t)\rangle = 0$ and correlation $\langle\eta_j(t)\eta_k(t')\rangle = \delta_{j,k}\delta(t-t')$, $\forall j,k \in \{1,2,...,N(t)\}$.

From Eq. (4) and from cell fate dynamics it is possible to derive the density equation and demonstrate that the homeostasis solution, ρ_{ss}, is indeed a linearly stable steady-state solution when neglecting the noise terms (see appendix).

We have considered three different motion dynamics. First we consider the simplest case by setting $u_{jk} = 0$ (NI cells). Secondly, it is studied the case in which cells

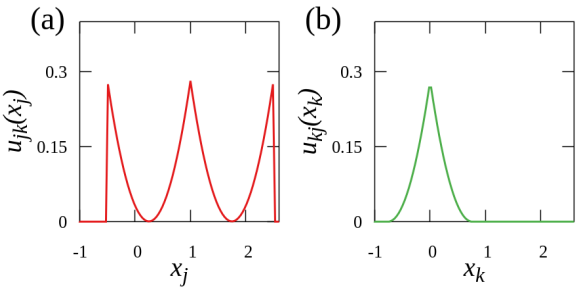

FIG. 1: (a) Adhesive potential (Eq. 6) generated by an adult cell (i.e. $l_k(t) = l_0$) at $x = 1$ to a newborn cell (i.e. $l_j(t) = l_0/2$) at position x_j. (b) Adhesive potential (Eq. 6) generated by a newborn cell at $x = 0$ to an adult cell at position x_k. As could be seen, $u_{jk} \neq u_{kj}$ for the adhesive potential.

interact through a pairwise harmonic potential (GM coupling). Defining $x_{jk} := |x_j - x_k|$,

$$u_{jk}(x_{jk}) = \frac{K}{2}(x_{jk} - d_{jk}^{eq})^2 \tag{5}$$

with K being the potential's strength, which its inverse determines the relaxation time, d_{jk}^{eq} being the equilibrium distance between cells j and k, which is regarded as $d_{jk}^{eq} := [l_j(t) + l_k(t)]/2$. The equilibrium distance is defined in a way that both cells tend to be in contact but without overlapping. It is worth noting that this harmonic potential increases for large x_{jk} so cells will move long distances if needed, generating cell migrations.

Third, to simulate cell adhesion (GA coupling) we short-ranged the pair-wise potential expressed in Eq. (5) as

$$u_{jk}(x_{jk}) = \frac{K}{2}(x_{jk} - d_{jk}^{eq})^2 \cdot \theta(d_k^c - x_{jk}), \tag{6}$$

where the equilibrium distance is the same as in the long-range potential (5), $\theta(x)$ is the Heaviside step function and d_k^c is the cutoff distance, defined as $d_k^c := 3l_k(t)/2$. As the cutoff distance varies with the size of the neighbouring cell, the adhesive force of an adult cell affect a larger range that the adhesive force of a growing one, which is smaller. Additionally, as the cutoff distance depends only on the k-th cell, $u_{jk} \neq u_{kj}$, as could be seen in Fig. 1. This adhesive potential allows us to generate a similar cell-cell interaction than in the long-range case (GM) but avoiding cellular migration, which we will see that is a relevant factor.

3. Numerical simulation

To simulate the different behaviours (CBD, VM and density feedback) we have tried to approach the system similarly to a clonal labeling experiment [5–8]. As a consequence, we have considered a 1-dim array of cells with periodic boundary conditions (ring) and positions $\{x_j(t)\}_{j=1}^{N(t)}$ with $N(t = 0) = N_{ini}$. Additionally, in

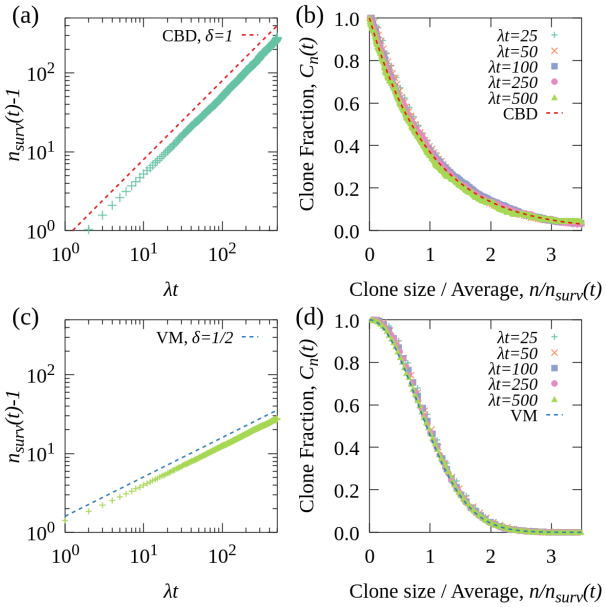

FIG. 2: Results obtained from the simulation of the canonical examples. (a) and (b) are the average clone size and the clone size distributions, respectively, for the CBD model. (c) and (d) are the average clone size and the clone size distributions, respectively, for the VM. The results are consistent with the expected statistics.

the feedback model simulations, the initial local density is $\rho_L(x; t = 0) = \rho_{ini} \neq \rho_{ss}$, $\forall x \in [0, L_{sys})$, where $L_{sys} := N_{ini}/\rho_{ini}$. We assume that all stem cells are equal and that the irreversible nature of cell differentiation could be modeled as an stochastic exclusion of the niche [9]. The algorithms used begin with one labeled cell and track its clone (i.e. the remaining labeled descendants) until it occupies the whole system or until its extinction. The number of labeled cells at a certain time is referred as $n_{surv}(t)$ and the clone size distribution as $C_n(t)$.

The numerical parameters are set as: $L = 40$, $t_{cell} = 200$, $t_{gr} = 0.1\, t_{cell}$, $N_{ini} = 500$, $l_0 = 1$, $\rho_{ini} = 0.95\, \rho_{ss}$, $\rho_c = 4.2$, $r = 0.3$ and $K = 1$. Equations (3) and (4) are discretized and numerically solved by the Euler-Maruyama method with $\Delta t = 0.05$. All results are calculated with 10^5 independent runs.

It is worth mentioning that all programs used to simulate the system have been build from scratch.

III. RESULTS AND DISCUSSION

We now discuss the numerical results. As it is shown in Fig. (2) the simulations of the CBD and VM models exhibit the expected statistics. Notably, the clone size distributions (Fig. 2(b) and 2(c)) and the δ exponents remain constant along time.

Fig. 3 shows the results obtained with NI dynamics. In both Figs. 3.(a) and 3.(c), the average clone size grows

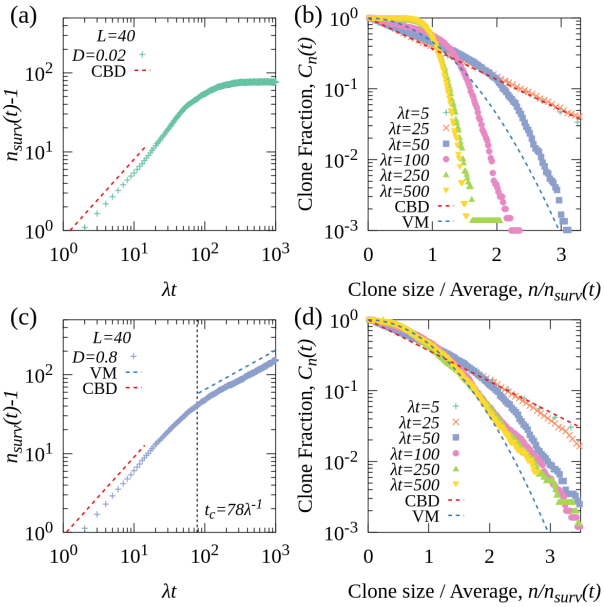

FIG. 3: Numerical results of the simulations with non-interacting (NI) dynamics. (a) and (b) are the average clone size and clone size distribution for $D = 0.02$, respectively. They show clustering since $t \sim 100t_{cell}$. (c) and (d) are the average clone size and clone size distribution for $D = 0.02$, respectively, which show VM emergence for $t > t_c$.

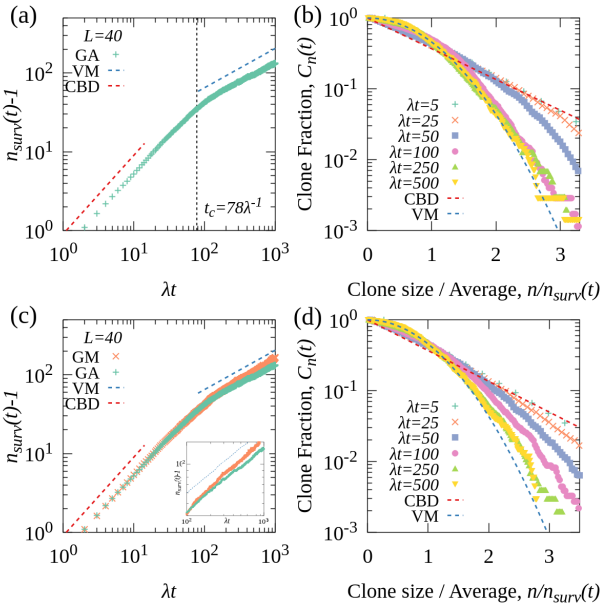

FIG. 4: Numerical results of the simulations with GA and GM coupling dynamics. (a) and (b) are the average clone size and clone size distribution for GA dynamics, respectively. GA shows VM emergence for $t > t_c$. (c) and (d) are the average clone size and clone size distribution for GD dynamics, respectively. As can be seen in the inset, GM statistics do not present VM emergence. In (c), results of GA dynamics are included for compairson.

linearly at short time scales (CBD statistics). However, in the large time scale, average clone size of NI dynamics with $D = 0.02$, Fig. 3.(a) shows stagnation. Looking at Fig. 3(b), its corresponding clone size distribution transitions to a step distribution indicating that the probability of finding clones with more than one cell is very low, so the labeled cell population shows clustering. We consider this an example of the Brownian bug problem, which has been observed in some models with self-replication and diffusion [9, 16]. To avoid this phenomenon, we set a higher diffusion constant ($D = 0.8$) so cells have larger motility avoiding cluster formation. In this situation of homogeneous clones, Figs. 3(c) and 3(d), we observe VM emergence at high time and length scales.

The numerical results obtained in the simulations with GA coupling and GM coupling dynamics are presented in Fig. 4. In both cases, $D = 0.02$ since GM and GA dynamics generate repulsion between cells avoiding clustering. Figs. 4(a) and 4(b) show a CBD behaviour at short times and VM emergence at large length and time scales. In Fig. 4(b) it is possible to see that the clone size distributions rapidly converge to the VM clone size distribution. On the other hand, Figs. 4(c) and 4(d) follow the CBD statistics at short times, but do not show VM emergence. As could be seen in the inset at Fig. 4(c), the average clone sizes grows faster than in the GA case. Additionally we observe at Fig. 4(d) that the clone size distribution converges slowly than in the GA case and do not seem to transition to the VM distribution.

The transition between CBD and VM takes place as a consequence of the competition between two length scales, the average clone size, $l_0 n_{surv}(t)$, and the interaction length L. As [9] proposed, we could observe the VM emergence when the average clone size exceeds the interaction length, L. Since the clone size statistics below that threshold are CBD statistics, we could estimate the transition time, t_c, from the following expression

$$L \approx l_0 n_{surv}(t_c) \approx l_{CBD}(t_c) = l_0 \left(1 + \frac{1}{2}\frac{t_c}{t_{cell}}\right), \qquad (7)$$

where the average clone size is approximated by the result of the CBD statistics. This way, $t_c = 2t_{cell}(L - l_0)/l_0$, that computed at $L = 40$, gives us a time $t_c = 78t_{cell}$.

In the short time scale, the cell fate is effectively regulated by global cell density, so the clone behaves as the CBD model. Otherwise, at large time scales ($t > t_c$) clone dynamics converge to the VM. Since the average clone sizes reaches L, the density feedback compensates the bulk fluctuations and the clone size fluctuations are driven by the fluctuations at the labeled clone surface, leading to the VM statistics [13], as could be seen in Fig. 5. We think that this is the reason by which the VM model emerges with short-ranged dynamics while with long-ranged ones, as the GM, the system responds to any fluctuation by globally relaxing so long-range interactions weaken the density feedback compensation of the bulk fluctuations and the VM does not emerge.

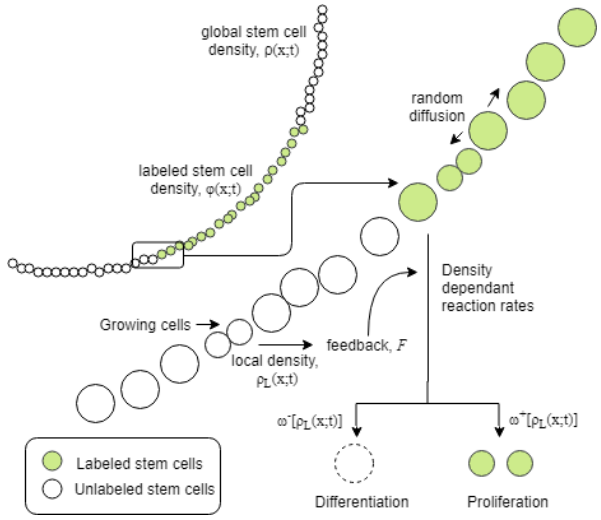

FIG. 5: Schematic view of the local density feedback dynamics. Homeostasis is maintained in the 1-dim tissue (ring) as a collective phenomenon in a population of stem cells. The diagram shows the interface between genetically labeled stem cells (green) and unlabeled ones (white), which is the zone that generates $n_{surv}(t)$ fluctuations in the VM kinetics.

IV. CONCLUSIONS

We presented a version of the stochastic cell fate decision model proposed in [9, 13] in which we added growth and long-range interactions. This model unifies the two previous stochastic models of homeostasis (CBD and VM) by the competition between the average clone size, $l_0 n_{surv}(t)$, and the interaction range, L.

We have found that, independently of the motion dynamics considered, the clones evolve as the CBD at short time and length scales as well as show VM emergence at large length and time scales, in agreement with [9, 13], for short-ranged dynamics. We have also estimated the transition time, t_c, as in [9]. It is important to note that at single cell level, cells always follow CBD dynamics since the VM dynamics emerge as a collective phenomenon at large length and time scales via the density feedback compensation of the bulk noise [13].

Long-range dynamics (GM) do not show VM emergence. We think that is due to them globally relaxing the system and weakening the bulk fluctuations compensation that generate the VM emergence.

Although the molecular mechanisms that lead to tissue homeostasis have not yet been discovered, our study helps to understand under which conditions the VM dynamics could emerge in 1-dim tissues. This conditions are, namely: stochastic cell-fate decisions, the presence of a feedback loop and short-ranged dynamics.

Acknowledgments

I would like to specially thank my advisor Marta Ibañes, to believe in this project and to be a guide in the difficulties. I would also like to thank my family, and specially to Júlia, to always listen and encourage me.

[1] Watt, F. M. and Hogan, B.L., *Out of Eden: Stem Cells and Their Niches*. Science **287**, 1427-1430 (2000).
[2] Klein, A. M. and Simons B. D., *Universal patterns of stem cell fate in cycling adult tissues*. Development **138**, 3103-3111 (2011).
[3] Potten, C. S. and Loeffler, M., *Stem cells: attributes, cycles, spirals, pitfalls and uncertainties. Lessons for and from the crypt*. Development **110**, 1001-1020 (1990).
[4] Knoblich, J. A., *Mechanisms of asymmetric stem cell division*. Cell **132**, 583-597 (2008).
[5] Lopez-Garcia, C., Klein, A. M., Simons, B. D. and Winton, D. J., *Intestinal stem cell replacement follows a pattern of neutral drift*. Science **330**, 822-825 (2010).
[6] Klein, A. M., Nakagawa, T., Ichikawa, R., Yoshida, S. and Simons, B. D., *Mouse germ line stem cells undergo rapid and stochastic turnover*. Cell Stem Cell **7**, 214-224 (2010).
[7] Jones, K.B. et al., *Quantitative Clonal Analysis and Single-Cell Transcriptomics Reveal Division Kinetics, Hierarchy, and Fate of Oral Epithelial Progenitor Cells*. Cell Stem Cell **24**, 183-192 (2019).
[8] Klein A. M., Doupé D. P., Jones P. H. and Simons B. D., *Kinetics of cell division in epidermal maintenance*. Phys. Rev. E **76**, 021910 (2007).
[9] Yamaguchi, H., Kawaguchi, K., and Sagawa T., *Dynamical crossover in a stochastic model of cell fate decision*. Phys. Rev. E **96**, 012401 (2017).
[10] Harris, T. E., *The Theory of branching processes*, (Springer, Berlin 1963, 1st. ed.).
[11] Dornic, I., Chat, H., Chave, J., and Hinrichsen, H., *Critical Coarsening without Surface Tension: The Universality Class of the Voter Model*. Phys. Rev. Lett. **87**, 045701 (2001).
[12] Holley, R. A. and Liggett,T. M., *Ergodic Theorems for Weakly Interacting Infinite Systems and the Voter Model* Ann. Probab. **3**, 643-663 (1975).
[13] Yamaguchi, H. and Kawaguchi, K., *Universal voter model emergence in genetically labeled homeostatic tissues*. arXiv 1903.02985v1 (2019).
[14] Sawyer, S., *Results for the Stepping Stone Model for Migration in Population Genetics*. Ann. Probab. **4**, 699-728 (1976).
[15] Basan, M.,Risler, T., Joanny, J.F., Sastre-Garau, X. and Prost, J., *Homeostatic competition drives tumor growth and metastasis nucleation*. HSFP J.**3**, 265272 (2009).
[16] Hernández-García, E. and López, C., *Clustering, advection, and patterns in a model of population dynamics with neighborhood-dependent rates*. Phys. Rev. E **70**, 016216 (2004).
[17] Dean,D. S., "Langevin equation for the density of a system of interacting Langevin processes". J. Phys. A: Math. Gen. **29**, L613 (1996).

APPENDIX: Density equation derivation

The global density is defined as $\rho(\mathbf{x}) := \sum_{j=1}^{N(t)} \rho_j(\mathbf{x})$, where $\rho_j(\mathbf{x}) = \delta(x - x_j(t))$ is the single-cell density, in terms of the space-time coordinate $\mathbf{x} = (x; t)$, and $\delta(x)$ is the Dirac delta function. Its evolution equation is obtained form Eq. (4) and from cell fate dynamics as in [9, 13, 17]. Consider an arbitrary function f which, from the definition of the single-cell density can be expressed as

$$f(x_j(t)) = \int \mathrm{d}x \rho_j(x; t) f(x). \tag{A1}$$

Differentiating it using Itô calculus and integrating by parts:

$$\begin{aligned}\frac{\mathrm{d}f}{\mathrm{d}t} =& \int \mathrm{d}x\, \rho_j \left[\frac{\mathrm{d}f}{\mathrm{d}x}\sqrt{2D}\eta_j(t) - \frac{\mathrm{d}f}{\mathrm{d}x}\frac{\partial U}{\partial x} + D\frac{\mathrm{d}^2 f}{\mathrm{d}x^2}\right] \\ =& \int \mathrm{d}x\, f\left[-\frac{\partial \rho_j}{\partial x}\sqrt{2D}\eta_j(t) + \frac{\partial \rho_j}{\partial x}\frac{\partial U}{\partial x} + D\frac{\partial^2 \rho_j}{\partial x^2}\right]. \end{aligned} \tag{A2}$$

Considering that $\mathrm{d}_t f = \int \mathrm{d}x\, \partial_t \rho_j(\mathbf{x}) f(x)$, where d_t and ∂_t denote total and partial differentiation respect to t, respectively,

$$\frac{\partial \rho_j}{\partial t} = -\frac{\partial}{\partial x}(\sqrt{2D}\rho_j \eta_j(t)) + \frac{\partial \rho_j}{\partial x}\frac{\partial U}{\partial x} + D\frac{\partial^2 \rho_j}{\partial x^2}. \tag{A3}$$

Now we could consider the cell fate dynamics of a single cell, which adds the term

$$B_j(\rho_j, \rho_L) = \Delta\omega(\rho_L)\rho_j(\mathbf{x}) + \sqrt{g(\rho_L)\rho_j}\, b_j(\mathbf{x}). \tag{A4}$$

Here, $\Delta\omega[\rho_L(\mathbf{x})] := \omega^+[\rho_L(\mathbf{x})] - \omega^-[\rho_L(\mathbf{x})]$ express the density increase/decrease due to a proliferation/differentiation process and $g[\rho_L(\mathbf{x})] := \omega^+[\rho_L(\mathbf{x})] + \omega^-[\rho_L(\mathbf{x})]$ is the fluctuation that it generates. Also, $b_j(\mathbf{x})$ is a white Gaussian noise term with correlation $\langle b_j(\mathbf{x}) b_k(\mathbf{x})\rangle = \delta_{j,k}\delta(\mathbf{x} - \mathbf{x}')$.

Combining Eq. (A3) and (A4) and summing for each j one obtains the expression

$$\begin{aligned}\frac{\partial \rho}{\partial t} &= D\frac{\partial^2 \rho}{\partial x^2} + \Delta\omega[\rho_L(\mathbf{x})]\rho(\mathbf{x}) + \frac{\partial}{\partial x}\left[\rho(\mathbf{x})\left(\frac{\mathrm{d}u}{\mathrm{d}x} * \rho\right)\right] \\ &+ \sum_{j=1}^{N(t)}\left[\sqrt{g(\rho_L)\rho_j}\, b_j(\mathbf{x}) - \frac{\partial}{\partial x}(\sqrt{2D}\rho_j \eta_j(t))\right], \end{aligned} \tag{A5}$$

where $*$ denotes convolution. To preserve the properties of a Markovian equation for the global density one could redefine the noise as in [13, 17],

$$\xi_\rho(\mathbf{x}) := \sum_{j=1}^{N(t)}\left[\sqrt{g(\rho_L)\rho_j}\, b_j(\mathbf{x}) - \frac{\partial}{\partial x}\sqrt{2D\rho_j}\, \eta_j(t)\right] \tag{A6}$$

which is a white Gaussian noise with correlation

$$\langle \xi_\rho(\mathbf{x})\xi_\rho(\mathbf{x}')\rangle = (g(\rho_L) + 2D\partial_x\partial_{x'})\, \rho(\mathbf{x})\delta(\mathbf{x} - \mathbf{x}'). \tag{A7}$$

Defining the density feedback, which expresses the contribution of proliferation-differentiation kinetics as well as cell-cell interactions, as $F(\rho_L, \rho) = \Delta\omega(\rho_L)\rho(\mathbf{x}) + \partial_x[\rho(\mathbf{x})(\mathrm{d}_x u * \rho)(\mathbf{x})]$ and considering the noise expression (A6), Eq. (A5) becomes

$$\frac{\partial}{\partial t}\rho(\mathbf{x}) = D\frac{\partial^2}{\partial x^2}\rho(\mathbf{x}) + F[\rho_L(\mathbf{x}), \rho(\mathbf{x})] + \xi_\rho(\mathbf{x}). \tag{A8}$$

The homeostasis solution, $\rho(\mathbf{x}) = \rho_{ss}$ corresponds to a linearly stable steady-state solution according to the analysis I have reproduced [13].